Published in final edited form as:
*Magn Reson Med*. 2011 December ; 66(6): 1722–1730. doi:10.1002/mrm.22968.

# Quantitative Tissue Oxygen Measurement in Multiple Organs Using $^{19}$F MRI in a Rat Model

**Siyuan Liu, PhD**[1,2], **Sameer J. Shah, MD**[2], **Lisa J. Wilmes, PhD**[1], **John Feiner, MD**[2], **Vikram D. Kodibagkar, PhD**[3], **Michael F. Wendland, PhD**[1], **Ralph P. Mason, PhD**[3], **Nola Hylton, PhD**[1], **Harriet W. Hopf, MD**[4], and **Mark D. Rollins, MD PhD**[2]

[1]Department of Radiology and Biomedical Imaging, University of California, San Francisco, CA, USA

[2]Department of Anesthesia and Perioperative Care, University of California, San Francisco, CA, USA

[3]Department of Radiology, University of Texas Southwestern Medical Center, Dallas, TX, USA

[4]Department of Anesthesiology, University of Utah, Salt Lake City, UT, USA

## Abstract

Measurement of individual organ tissue oxygen levels can provide information to help evaluate and optimize medical interventions in many areas including wound healing, resuscitation strategies, and cancer therapeutics. Echo planar $^{19}$F MRI has previously focused on tumor oxygen measurement at low oxygen levels ($pO_2$) < 30 mmHg. It uses the linear relationship between spin-lattice relaxation rate ($R_1$) of hexafluorobenzene (HFB) and $pO_2$. The feasibility of this technique for a wider range of $pO_2$ values and individual organ tissue $pO_2$ measurement was investigated in a rat model. Spin-lattice relaxation times ($T_1=1/R_1$) of HFB were measured using $^{19}$F saturation recovery echo planar imaging (EPI). Initial *in vitro* studies validated the linear relationship between $R_1$ and $pO_2$ from 0 mmHg to 760 mmHg oxygen partial pressure at 25°C, 37°C, and 41°C at 7 Tesla for HFB. *In vivo* experiments measured rat tissue oxygen ($ptO_2$) levels of brain, kidney, liver, gut, muscle and skin during inhalation of both 30% and 100% oxygen. All organ $ptO_2$ values significantly increased with hyperoxia ($p<0.001$). This study demonstrates that $^{19}$F MRI of HFB offers a feasible tool to measure regional $ptO_2$ *in vivo*, and that hyperoxia significantly increases $ptO_2$ of multiple organs in a rat model.

### Keywords

oximetry; tissue oxygen tension; fluorine MRI; hexafluorobenzene

## Introduction

The primary goal in treating critically ill patients is to ensure adequate perfusion and oxygenation of vital organs. Tissue oxygenation is complex and depends upon the interaction of blood flow, arterial oxygen tension, hemoglobin dissociation conditions, oxygen carrying capacity, mass transfer resistances and local oxygen consumption. Tissue hypoxia has a high correlation with organ failure and poor prognosis in severe disease states(1,2). Frequently used surrogates for tissue oxygenation include blood pressure, heart

**Corresponding author:** Mark D. Rollins, MD, PhD, UCSF, Department of Anesthesia and Perioperative Care, 513 Parnassus Avenue, S-455, UCSF Box 0464, San Francisco, CA 94143-0464, Tel: 415-476-1195, Fax: 415-476-1623, RollinsM@anesthesia.ucsf.edu.

rate, cardiac filling pressures, cardiac output, hemoglobin saturation, systemic blood gas measurement, and lactate levels. All are global measures and give no specific information about the status of individual organs. Abnormal values of these surrogate measures often signify a poor prognosis. However, using medical therapies to obtain normal values does not reliably predict a favorable result, and may lead to patient outcomes that are worse, better, or unchanged(3). Measurement of individual organ tissue oxygen levels could help physicians and investigators evaluate and optimize medical interventions in many areas including wound healing(4), resuscitation strategies(5), and cancer therapeutics(6) by providing defined endpoints to titrate therapies and evaluate interventions.

A variety of tissue oxygen measurement techniques exist, but all have limitations. Although polarographic electrodes are considered the gold standard of oximetry, they are invasive, consume oxygen, sample a limited tissue volume, and cannot display the heterogeneity of tissue oxygen levels(7). Although fiberoptic probes do not consume oxygen, they suffer from similar limitations regarding invasiveness and fragility(8). Methods based on hemoglobin (Hb) saturation, such as near infrared spectroscopy, measure an average of arterial, venous, and capillary blood in a large tissue volume. Electron paramagnetic resonance (EPR) gives precise tissue oxygen values and allows repeated measurements, but requires implantation of a paramagnetic material, is limited in its sampling area, and is hindered by a lack of available instrumentation(9). Positron emission tomography images tissue oxygen levels using intravenous reporter molecules that become trapped in the tissues, but the calibration range of this method is limited to hypoxic conditions(10). Blood oxygen level-dependent (BOLD) MRI is sensitive to intravascular Hb saturation but does not provide absolute $pO_2$. Although the BOLD technique is positively correlated with tumor $pO_2$, its intravascular based imaging does not reliably predict tissue $pO_2$(11,12). In addition, it is heavily affected by changes in blood flow and vascular volume(13).

A quantitative oximetry method using fluorine-based MRI has been developed that allows regional dynamic changes to be measured from sequential images of tissue oxygen(14,15). The use of $^{19}F$ MRI oximetry based on direct tissue injection of hexafluorobenzene (HFB) has primarily been directed at measurements of tumor oxygenation in animal models, and has consequently focused on $pO_2$ quantitative imaging at low oxygen levels(16). We have chosen this method because it is minimally invasive, requiring only microliters of a fluorinated substance to be injected, it directly measures $pO_2$ in the tissue, allows imaging of regional tissue oxygen distributions based on small voxels (typically, in-plane areas of 1.25 mm X 1.25 mm), and has been validated by direct comparison to multiple polarographic electrode measurements(7,15,16) and fluorescence quenching oximetry(17). Various perfluorocarbons (PFCs) have served as reporter molecules, each exhibiting a linear relationship between their corresponding spin lattice relaxation rate ($R_1$) and $pO_2$(18). The ability of a PFC to measure $pO_2$ varies with its molecular properties and route of administration. PFCs injected intravenously tend to be largely sequestered by the reticuloendothelial system into the liver and spleen(19). This method of administration often results in levels of PFC accumulation in other tissues of interest that are too low to provide an adequate signal to noise ratio (SNR). Additionally, intravenous administration has the potential to produce even lower tissue concentrations of PFC in poorly vascularized regions. Even though the technique is not dependent on absolute reporter molecule concentration, these areas would have a SNR too low for accurate $pO_2$ measurement, and could bias the technique to areas of higher perfusion and oxygenation. In contrast, the technique of direct tissue injection affords greater precision and sensitivity of $pO_2$ measurements, as well as the ability to study potentially poorly perfused areas(20,21). The PFC hexafluorobenzene (HFB) has 6 magnetically equivalent fluorine atoms, resulting in a single resonance. This feature provides high sensitivity, an advantageous SNR, and dramatically simplifies imaging. HFB also has the advantage of a relatively low sensitivity to both temperature and pH variation,

and is easily available through several commercial sources(15,22). HFB has minimal toxicity, with no mutagenicity, teratogenicity, or fetotoxicity reported, and an LD50 > 10g/kg when administered orally or intraperitoneally in rats(20). Thus HFB also has the potential for future use in humans.

Although the vast majority of oxygen content in blood is carried on hemoglobin, increasing inspired oxygen levels results in a significant increase in arterial plasma oxygen content (dissolved oxygen), and is associated with improved wound healing, decreased infection rates, and improved efficacy of cancer treatment(23,24). High levels of inspired oxygen (ranging up to 100%) are used daily in the operating rooms and critical care units to improve arterial oxygenation, although the effects on tissue oxygenation are not normally measured in the clinical setting. Even under normobaric conditions, high oxygen tension in the arterial blood has been reported to lead to hemodynamic changes including bradycardia, decreases in both pulmonary artery pressure and cardiac output, and increases in systemic vascular tone(25,26). Despite many attempts, animal studies have generally failed to identify specific organs or tissue areas of altered blood flow during hyperoxia. An increase in vascular resistance from hyperoxia has been observed in animal models, but blood flow to major organs appeared to be preserved(27–29). The specific mechanisms of both changes in vascular resistance and changes in tissue oxygen consumption remain unknown, leaving the regional effects of hyperoxia unclear, and highlighting the need for direct tissue oxygen measurement.

A better understanding of how hyperoxia affects individual organ oxygenation is needed to optimize the use of oxygen as a medical therapy. Therefore, one of the goals of this study was to examine the influence of increasing the dissolved arterial oxygen content on individual organ $pO_2$ as measured by $^{19}F$ MRI, while ensuring that temperature, arterial $CO_2$, anesthetic depth, and intravascular volume status remained constant. For this study, we chose inspired oxygen levels that would ensure a nearly complete saturation of hemoglobin, yet provide markedly different arterial blood $pO_2$. To examine the influence of hyperoxemia on individual organs, we measured brain, gut, kidney, liver, muscle, and skin oxygen tension during ventilation with the fraction of inspired oxygen ($FiO_2$) set at either 0.3 or 1.0 in a euthermic, euvolemic, anesthetized rat model. An $FiO_2$ of 0.3 rather than room air (0.21) was chosen because under general anesthesia there is an increase in pulmonary shunting which results in hypoxic arterial oxygen levels compared to awake subjects. In addition, an $FiO_2$ of less than 0.3 is rarely used in either the intensive care unit (ICU) or operating room for patients that are intubated and anesthetized.

## Methods

### Magnetic Resonance Pulse Sequence for Measuring the $T_1$ of HFB

A saturation recovery echo planar imaging (EPI) sequence(15) was used to measure the $T_1$ of directly injected HFB. A group of twenty 90° hard pulses with 50 ms spacing was applied to saturate the magnetization along the z-axis. Following a variable time delay (τ), a single-shot spin echo with blipped phase encoding EPI was used to collect images. The saturation recovery was favored, and chosen over the traditional inversion recovery since there is no need to wait more than a period of $5T_1$ between acquisitions for longitudinal relaxation recovery. This method is well suited for long $T_1$ measurements, which were common in this study. The Alternated Relaxation Delays with Variable Acquisitions (ARDVARC) scheme (30) was modified and used to acquire 14 τ in the order: 90 s, 200 ms, 60 s, 400 ms, 40 s, 600 ms, 20 s, 800 ms, 16 s, 1 s, 8 s, 1.5 s, 4 s, and 2 s. This acquisition scheme is optimized to minimize any error from the clearance effects of HFB *in vivo*. A wide range of τ values was selected since the range of the expected $T_1$ values under differing oxygen conditions is broad. Generally, the corresponding number of averages was set to one for all delays, but

occasionally an average of two was needed when the signal-to-noise ratio (SNR) was low. The acquisition time per $T_1$ measurement was approximately 5 minutes. The standard voxel size was 1.25 × 1.25 × 5 mm.

### Calibration of HFB $R_1$ and $pO_2$ at 7 Tesla

Calibration techniques were based on previously described methods used at 4.7T magnetic field strength(15,30). Three different HFB samples were equilibrated at each of 5 different oxygen concentrations balanced with nitrogen. The concentrations examined were 0% $O_2$ (pure $N_2$), 5% $O_2$, 10% $O_2$, 21% $O_2$, 50% $O_2$, 100% $O_2$. These oxygen concentrations were examined under atmospheric pressure (sea level) at 25°C, 37°C, and 41°C. Additionally, since 2% isoflurane was used to anesthetize animals, the entire calibration sample conditions were repeated with and without the presence of 2% isoflurane in order to determine whether the fluorine atoms in isoflurane affect the linear relationship between the $R_1$ of HFB and $pO_2$. The $pO_2$ was calculated using standard partial pressure equations taking into account the barometric pressure, oxygen percentage, temperature, and presence of water vapor(31).

One ml of HFB was added to a gas-tight NMR tube (Wilmad Lab Glass, Buena, NJ, USA) together with 5 ml water. Since HFB is hydrophobic and immiscible with water, the denser HFB remained in a separate layer at the bottom of the tube. The NMR tube containing HFB and water was equilibrated under the desired temperature and atmospheric conditions within a sealed previously equilibrated chamber using a small catheter with the selected gas continuously bubbled into the sample. The desired temperature was maintained during imaging using a water bath containing $D_2O$ circulating in tubing surrounding the NMR tube. The $T_1$ of HFB in the sample was then determined with $^{19}F$ saturation recovery EPI. The experiment was repeated in triplicate for each oxygen and temperature condition of interest. Separate sets of experiments determined the time needed for oxygen equilibration in this experimental set-up and confirmed maintenance of a constant selected temperature during imaging.

### Animal preparation

The University of California, San Francisco Institutional Animal Care and Use Committee (IACUC) approved this work and animal protocol prior to any experimentation. Twelve male Sprague-Dawley rats (250–350g, Charles River Labs, Wilmington, MA, USA) were anesthetized with isoflurane. General anesthesia was initially maintained with 2.0% isoflurane in 100% oxygen via nose cone during placement of invasive monitoring and HFB. The rat was shaved, and placed on an adjustable temperature water pad, which was used to keep the animal euthermic (37.5 °C ± 0.5°C). Temperature was measured by rectal probe. An MRI compatible pulse oximeter (Nonin Medical, Inc. Plymouth, MN) was placed on the animal's right hind paw; heart rate and oxygen saturation were monitored for the duration of the experiment. The trachea was exposed and a tracheal ventilation cannula placed and secured. The rat was then mechanically ventilated throughout the experiment in order to control and maintain normal physiologic arterial $CO_2$ levels and decrease atelectasis during the experiment. Initial ventilation settings of 70 breaths/min and tidal volume of 12 ml/kg were then adjusted based on end tidal carbon dioxide, which was monitored every 15 minutes throughout the remainder of the surgery and experimental procedure. These higher tidal volume settings were necessary due to the large capacitance in the longer length of tubing needed to position the ventilator outside the magnetic field of the scanner. Following the tracheotomy, the femoral artery was cannulated. A 1.5 cm incision was made along the crease formed by the abdomen and left thigh (contralateral to the side with the pulse oximeter). The femoral artery was then exposed. Approximately 1 cm of the vessel was dissected free under microscopic visualization and a saline-filled catheter inserted into the vessel and secured in place with suture. This arterial line was then connected to a blood

pressure monitor (Spacelabs Healthcare, Issaquah, WA, USA) and used throughout the remainder of the preparation and data collection for blood pressure monitoring and blood gas sampling. After securing the arterial line, the tail vein was cannulated with a 24 gauge catheter and attached to a programmable syringe infusion pump (New Era Pump Systems, Inc., Wantagh, NY, USA); 10mL/kg normal saline was bolused at this time to replace losses during surgery, and then normal saline infused intravenously at a rate of 2.5mL/kg/hr for fluid maintenance. Total surgical time ranged from 60 to 120 minutes.

The animal was placed on its side, and a superficial skin nick (2mm) was made on the proximal hind thigh, contralateral to the arterial cannulation. Aliquots of HFB were injected into multiple tissues of each rat as follows: 50 μL HFB was incrementally injected under direct vision into the muscle with a 33 ga. needle. Percutaneous injection was used for placement of 50 μL HFB into the skin. Following a small scalp incision, a 1.5 mm diameter hole was drilled through the animal's skull, 2mm anterior to the bregma and 4mm lateral from midline. 30 μL HFB was injected 1.5 mm below the dural layer over 10 minutes with the assistance of a stereotactic frame and microscope. A 1.5 to 2.0 cm incision was made just caudal to the right inferior costal margin, through the peritoneum to expose the kidney, liver, and gut. 50 μL HFB was injected into the liver tissue, kidney tissue, and gut wall under direct vision. Total time for HFB injection for all organs of interest was approximately 60 minutes.

## MRI Experiments

All experiments were performed on a Varian DirectDrive™ 7T horizontal bore magnet equipped with 21-cm inner diameter imaging gradients that provide ±200 mT/m (Varian, Inc., Palo Alto, CA, USA). A custom constructed $^{19}F/^{1}H$ dually tunable birdcage RF transmit/receive coil (Rapid Biomedical GmbH, Rimpar, Germany) with 7.2 cm inner diameter was used for proton and fluorine imaging. Each animal was randomly assigned to an initial $FiO_2$ of 0.3 or 1.0. Following surgical preparation and HFB injection, the animal was allowed to equilibrate on the assigned $FiO_2$ for 20 minutes, and an arterial blood gas (ABG; 0.25 ml) was sampled and analyzed using an i-STAT® hand held blood analyzer (Abbott Point of Care, Inc., East Windsor, NJ, USA). The rat was kept prone on a $D_2O$ circulating warming pad and covered with a plastic covered cotton drape throughout the experimentation to maintain euthermia. The animal and monitoring lines were secured onto a custom built Plexiglas bed and cradle inserted into the magnet such that the RF coil center was aligned to the isocenter of the imaging gradients. The bed was manually adjusted to position each different organ location at the center of the RF coil. The order of imaging each organ of interest was randomized. Conventional $T_1$-weighted 2D spin echo $^{1}H$ and $^{19}F$ images with typical voxel size of 0.625×0.625×2 mm were acquired to identify the position of HFB signal for different organs of interest. Following the anatomical scans, the $T_1$ of the implanted HFB was measured with the saturation recovery EPI. The field of view (FOV) of the saturation recovery EPI images was the same as the spin echo images for appropriate signal registration.

Ventilation, administration of isoflurane, and continuous monitoring of pulse and blood pressure were continued throughout the MRI scan, with all ferrous metal monitors and equipment located outside the 5-gauss field line. Rectal temperature was recorded prior to placement of the rat in the magnet and again following completion of the scan. Abdominal images were acquired with respiratory gating. The respiration signal was determined using a mechanical pressure transduction signal from the ventilator exhaust outlet that was transferred into a respiratory gating module (Small Animal Instruments, Inc, Stony Brook, NY, USA).

Following the organ scans at the initial $FiO_2$, the inspired gas was changed to the alternate value. The animal was rescanned as described above after a 20-minute equilibration period. Following the scan, 0.25 ml of arterial blood was again taken for blood gas and hematocrit analysis. The total scan time for both $FiO_2$ values was approximately 2.5 hrs.

After completion of imaging, the animal was removed from the magnet, a final blood gas drawn, and the animal euthanized.

## Data Analysis

Raw data were imported into Matlab (MathWorks Inc., Natick, MA, USA) for image reconstruction and processing. The $T_1$ was calculated voxel by voxel in the selected region of interest (ROI) with a three-parameter fit using the Levenberg-Marquardt algorithm(32). Error estimates of the derived $T_1$ were calculated from the residuals and Jacobian matrix used in this fit method. The *in vitro* calibration data at each temperature were then fit to Eq. [1] as previously detailed by Zhao et al.(15):

$$R_1 = A + B * psO_2 \quad [1]$$

Where $R_1$ is the spin lattice relaxation rate ($s^{-1}$), $psO_2$ is the oxygen pressure in the sample (mmHg), A and B are constants at a given temperature and magnetic field. $R_1$ was derived from the reciprocal of the mean $T_1$ averaged over selected ROIs in three individual measurements.

Prior research has demonstrated a linear dependence of $R_1$ on temperature over a small range(33). Assuming a linear dependence of A and B with temperature T, then A= C+D*T and B= E+ F*T, and Eq. [1] is transferred into a temperature-dependent model described by Eq. [2]:

$$R_1 = C + D * T + (E + F * T) * psO_2 \quad [2]$$

where C, D, E, F are constants, T is the temperature in the unit of Celsius. These results were used to examine the effects of temperature at a field strength of 7T.

The *in vivo* tissue oxygen pressure ($ptO_2$) was calculated for each voxel in the selected ROI using the linear calibration equation derived at 37°C shown in Eq. [3] in the Results section. To improve data quality, similar to previous analysis methods(15), any voxels with calculated $T_1$ error greater than 40% (determined from the curve fit to derive $T_1$) were omitted from statistical analysis. In addition, any extreme outliers were also removed by combining voxels from all animals for a given condition, and removing voxels with $ptO_2$ outside the mean $ptO_2 \pm 2.5$SD. Application of these two criteria resulted in removal of 169 voxels and 21 voxels respectively from an original total of 1190.

## Statistical Analysis

Baseline physiologic rat data were compared between an $FiO_2$ of 0.3 and 1.0 using a paired t-test. A linear mixed effects model was used for statistical data analysis of $ptO_2$ as the primary study outcome, with condition ($FiO_2$ of 0.3 or 1.0) and organ as the two primary fixed effects. The entire data set was analyzed using a two-way repeated measures analysis of variance (ANOVA). Because we were specifically interested in different effects by organ, we tested all pair-wise differences in the regression-adjusted ("least squares") estimates of organ differences, using the post hoc Tukey-Kramer test to adjust for multiple comparisons. In addition, separate one-way ANOVA's were completed across organs for each inhaled

oxygen condition in order to alleviate the reduced power of the numerous multiple comparisons of the two-way ANOVA. All calculations were done using SAS/STAT software (Version 9.1.3 of the SAS System for Windows Copyright ® 2002–2003 and JMP 7.01, SAS Institute Inc., Cary, NC, USA). Under this study design, with a planned sample size of 12 and the anticipated effect size based on previously published values of rat organ $ptO_2$(9,34,35), our *a priori* power analysis determined that we should have > 85% power to detect a statistically significant difference with an alpha level set at 0.05 under the null hypothesis of no organ site difference.

## Results

### Calibration Results

No significant differences were found in sample calibration results (Table 1) with and without 2% isoflurane for a given temperature. Therefore only results of samples with the addition of 2% isoflurane are shown in Figure 1 to simulate the *in vivo* environment. The $T_1$ of HFB ranged from 9.8 s at 0% oxygen to 0.77 s at 100% oxygen at 37°C. The $R_1$ of HFB was linearly dependent on $pO_2$ from 0% oxygen to 100% oxygen at 25°C, 37°C and 41°C, shown in Figure 2. At 37°C, A = 0.1041 ± 0.0014 $s^{-1}$, B = 0.001659 ± 0.000004 (s mmHg)$^{-1}$ were derived with linear fit ($R^2$ = 0.99998) according to Eq. [1]. Thereby the calibration equation at 37°C can be written as follows:

$$pO_2(\text{mmHg}) = (R_1(s^{-1}) - 0.1041)/0.001659 \quad [3]$$

As shown in Figure 1, the HFB $R_1$ temperature dependence increased as $pO_2$ increased. Fitting the $R_1$ of HFB at different $pO_2$'s and temperatures to the temperature-dependent model Eq. [2] gave C = 0.1500 ± 0.0040 $s^{-1}$, D = −(1.21 ± 0.12) × $10^{-3}$ (s °C)$^{-1}$, E = (2.69 ± 0.06) × $10^{-3}$ (s mmHg)$^{-1}$, and F = −(2.74 ± 0.18) × $10^{-5}$ (s mmHg °C)$^{-1}$.

Figure 2 displays the calibration curve temperature dependence of both the intercept (2a) and slope (2b) with and without the presence of isoflurane.

### *In vivo* Results

The mean rat physiologic data from the *in vivo* experimentation are provided in Table 2. Mean arterial $pO_2$ was 98 ± 12 mmHg at an $FiO_2$ of 0.3 and 400 ± 85 mmHg at an $FiO_2$ of 1.0, reflecting the specific significant increase of dissolved oxygen in plasma due to the increase of $FiO_2$ ($p<.01$). No significant differences in the remaining measured physiologic data were noted. Mean arterial $CO_2$ was 38 ± 5 mmHg, mean Hb was 12.8 ± 0.9 g/dL. Both parameters remained in the physiological range throughout the *in vivo* experiments. Mean weight of 12 rats was 312 ± 39 grams. Core temperature of animals remained euthermic ranging from 37.0°C to 38.0°C during all experiments.

The distributions of $ptO_2$ in all six organs of interest at $FiO_2$ conditions of 0.3 and 1.0 are shown in Figure 3. These $^{19}F$ MRI based images are from a single representative animal. The shift towards yellow and orange colors displayed in the $ptO_2$ mapping on the right side represents higher values $ptO_2$ in all scanned organs at $FiO_2$ of 1.0 compared to 0.3. Separate organ histograms of the $ptO_2$ values recorded from all animals are displayed in Figure 4. Tissue oxygenation is heterogeneous in individual organs and is noted to vary significantly between organs at the higher level of inspired oxygen (FiO2 = 1.0).

Mean values of $ptO_2$ were calculated over all voxels in the selected ROI for each organ in each individual animal. The mean organ $ptO_2$ from all animals under each inspired oxygen condition are displayed graphically in Figure 5. The mean organ $ptO_2$ values at an $FiO_2$ of

0.3 ranged from 57 ±13 mmHg to 75 ± 15 mmHg. The mean organ $ptO_2$ values at an $FiO_2$ of 1.0 ranged from 127 ± 44 mmHg to 197 ± 86 mmHg. Our final mixed model (two-way ANOVA) showed both "condition" (p-value <.001) and "organ" (p-value <.001) to be significant predictors of $ptO_2$ level. For each organ studied, the $ptO_2$ measured with an $FiO_2$ = 1.0 was significantly greater than that measured while the animal was ventilated with an $FiO_2$ = 0.3 ($p < .05$). This result demonstrates a significant positive increase in organ $ptO_2$ values at the higher inspired oxygen condition. Comparison of organs showed that the subgroup $ptO_2$ values of skin and muscle were significantly greater than brain and gut which in turn were significantly greater than kidney and liver $ptO_2$ values ($p<.05$). A second analysis across organs using a one-way ANOVA at each $FiO_2$ condition found a significant organ $ptO_2$ difference noted with an $FiO_2$ = 1.0 (similar to the two-way ANOVA), but no significant difference between organ $ptO_2$ values at an $FiO_2$ =0.3.

## DISCUSSION

We demonstrated the feasibility of quantitative tissue oxygen mapping in a rat model with $^{19}F$ MRI measurement of directly injected HFB in multiple organs under two inspired oxygen conditions. Calibration results showed that the spin-lattice relaxation rate $R_1$ of HFB is linearly dependent on oxygen pressure $pO_2$ at a fixed temperature in the physiological range 25–41°C from 0% to 100% oxygen. Calibration Eq. [3] is similar to the calibration equation previously derived from 0% to 21% oxygen at 7T(22). The $R_1$ of HFB is highly sensitive to $pO_2$, but minimally sensitive to temperature. Since the rat core temperature was carefully maintained between 37°C and 38°C throughout *in vivo* experimentation, the error of $ptO_2$ measurement was minimized (6 mmHg/°C at $pO_2$ 300 mmHg). According to calibration results, 2% isoflurane used for anesthesia *in vivo* has no significant effects on the calibration equation, and consequently inhaled perfluorocarbon anesthetics can be used without worry of affecting the results of a $^{19}F$ MRI study using HFB. Prior studies demonstrated that the linear dependence of $R_1$ of PFCs on $pO_2$ is also essentially unresponsive to pH, $CO_2$, charged paramagnetic ions, mixing with blood, or emulsification(15,36). This allows $^{19}F$ MRI to remain a viable option for measuring $ptO_2$ under a variety of physiologic conditions.

The mean values of $ptO_2$ using $^{19}F$ MRI in this study are consistently somewhat higher than literature values previously reported for corresponding measurements of brain, kidney, and muscle in rats measured by EPR(9,34,35). The use of EPR $ptO_2$ measurement shows a similar significant rise in $ptO_2$ with increasing inspired oxygen concentration in measurement of both rat and mouse specific organs(9,34,37). The $^{19}F$ MRI oximetry values are also somewhat higher than previous rat organ measurements of $ptO_2$ obtained using polarographic electrodes(38–42). In a previous study by Jordan et al. using both $^{19}F$ MRI oximetry and fluorescence quenching fiber-optic probe oximetry to quantify the *in vivo* response of mouse tumor $pO_2$ with inhalation of carbogen, the tumor $pO_2$ determined with the $^{19}F$ MRI technique was typically higher(17). The exact reason for the higher absolute values with organ $ptO_2$ measurement using $^{19}F$ MRI compared to EPR, polarographic electrode, and fluorescence quenching measurements remains uncertain, but may be due to differences in tissue disruption, use of a mean of multiple measurement voxels (with $^{19}F$ MRI) vs. a single value averaging a larger area of contacting tissue, length of time between placement of reporter material and measurement, anesthetic technique, and control of specific variables known to change tissue perfusion such as temperature, volume status, and spontaneous vs. controlled ventilation. We observed that HFB signal was often imaged near the ventricular floor of the brain instead of cortex layer at the top in Fig. 3. We suspect that the HFB entered the cerebral spinal fluid (CSF) in either ventricles or subdural space in many studies despite a careful slow injection aided by a stereotactic syringe holder and microscope. The parenchymal injection is difficult to reliably reproduce as this layer in the

rat brain is approximately 1 – 2 mm thick and HFB will enter the CSF if the needle tip is either to shallow or deep, frequently traveling to the ventricle and sinking to the floor due to its hydrophobic nature and greater density than water. The failure of HFB injection in the parenchyma may overestimate brain tissue oxygen levels since $pO_2$ in CSF is often higher than in brain tissue itself(43).

The marked variability and different absolute increases in the organ $ptO_2$ noted in our study using $^{19}F$ MRI, show the diversities of oxygenation in various organs and the potential benefit of the regional versus global measurements this technique allows. The increased amount of oxygen bound to hemoglobin due to increasing the $FiO_2$ from 0.3 to 1.0 is small since both levels of corresponding arterial $pO_2$ (98 and 400 mmHg respectively) represent conditions in which hemoglobin is nearly fully saturated. However the mean arterial $pO_2$ at an $FiO_2$ of 1.0 was four fold higher than values corresponding to an $FiO_2$ of 0.3, which reflects the large increase of oxygen dissolved in plasma. Therefore, we conclude that the increases in $ptO_2$ quantified in all studied organs were primarily caused by the increased dissolved oxygen level in plasma. Although the increase in arterial blood oxygen content due to the increased $FiO_2$ is small when compared to the total oxygen content, the corresponding increase of arterial $pO_2$ tension significantly increases the driving force of oxygen diffusion from the capillary bed into tissue, and thus increases the absolute organ $ptO_2$. We believe the $^{19}F$ MRI technique does not reflect an unintended direct measure of the arterial $pO_2$, as all organ tissue values are significantly less than the arterial oxygen levels, and any HFB in direct contact with the vascular system would be rapidly removed from the tissue, taken to the lungs and exhaled.

Similar absolute increases of $ptO_2$ were found regardless of the order of inspired oxygen levels. This indicates that the tissue damage from the HFB injection was likely minimal. However, during the injection of HFB, transient reductions of blood pressure were observed occasionally. HFB has been used in the past as an inhaled anesthetic(44). These brief hypotensive episodes were most likely caused from a small portion of the HFB entering the intravascular compartment during the injection and exerting an anesthetic effect and its associated brief period of vasodilation or decreased myocardial contractility associated with most anesthetics. In order to prevent the transient acute blood pressure drop, we slowed the injection rate in each organ and reduced the isoflurane concentration briefly during the HFB injection period. The observed retention period of HFB was different in each organ. We believe that the residence time and clearance of HFB is most likely dependent on the individual organ perfusion. Half lives of HFB in less perfused organs such as muscle and skin are reported to be approximately 10 hours(18). HFB signal decayed faster in the more vascularized organs, *eg*. liver and kidney. The alternated relaxation delays were used to minimize the error in $T_1$ measurement that might otherwise result from the clearance effect of HFB. Two signal averages were used to compensate for the signal loss when a low SNR of HFB was a concern for MRI scans at later post-injection times.

In summary, this minimally invasive $^{19}F$ MRI oximetry technique using HFB as a reporter probe provides a sensitive quantitative method for measuring regional organ tissue oxygen tension and dynamic changes. These measures represent the balance between oxygen delivery and metabolic use, providing an endpoint to help guide future medical research and optimize a variety of therapeutic interventions, resuscitation strategies, and disease processes.

## Acknowledgments

Funding for this project was from the following sources:

1. Foundation for Anesthesia Education and Research

2. SW-SAIRP grant U24 CA126608

3. NIH grant R01 CA139043-01A1

## REFERENCES

1. Donati A, Loggi S, Preiser JC, Orsetti G, Munch C, Gabbanelli V, Pelaia P, Pietropaoli P. Goal-directed intraoperative therapy reduces morbidity and length of hospital stay in high-risk surgical patients. Chest. 2007; 132(6):1817–1824. [PubMed: 17925428]
2. Lima A, van Bommel J, Jansen TC, Ince C, Bakker J. Low tissue oxygen saturation at the end of early goal-directed therapy is associated with worse outcome in critically ill patients. Crit Care. 2009; 13 Suppl 5:S13. [PubMed: 19951385]
3. Boyd O, Grounds RM, Bennett ED. A randomized clinical trial of the effect of deliberate perioperative increase of oxygen delivery on mortality in high-risk surgical patients. JAMA. 1993; 270(22):2699–2707. [PubMed: 7907668]
4. Fife CE, Smart DR, Sheffield PJ, Hopf HW, Hawkins G, Clarke D. Transcutaneous oximetry in clinical practice: consensus statements from an expert panel based on evidence. Undersea Hyperb Med. 2009; 36(1):43–53. [PubMed: 19341127]
5. Wan JJ, Cohen MJ, Rosenthal G, Haitsma IK, Morabito DJ, Derugin N, Knudson MM, Manley GT. Refining resuscitation strategies using tissue oxygen and perfusion monitoring in critical organ beds. J Trauma. 2009; 66(2):353–357. [PubMed: 19204507]
6. Bache M, Kappler M, Said HM, Staab A, Vordermark D. Detection and specific targeting of hypoxic regions within solid tumors: current preclinical and clinical strategies. Curr Med Chem. 2008; 15(4):322–338. [PubMed: 18288988]
7. Mason RP, Hunjan S, Constantinescu A, Song Y, Zhao D, Hahn EW, Antich PP, Peschke P. Tumor oximetry: comparison of 19F MR EPI and electrodes. Adv Exp Med Biol. 2003; 530:19–27. [PubMed: 14562701]
8. Lubbers DW. Oxygen electrodes and optodes and their application in vivo. Adv Exp Med Biol. 1996; 388:13–34. [PubMed: 8798790]
9. Khan N, Williams BB, Hou H, Li H, Swartz HM. Repetitive tissue pO2 measurements by electron paramagnetic resonance oximetry: current status and future potential for experimental and clinical studies. Antioxid Redox Signal. 2007; 9(8):1169–1182. [PubMed: 17536960]
10. Chapman JD, Schneider RF, Urbain JL, Hanks GE. Single-photon emission computed tomography and positron-emission tomography assays for tissue oxygenation. Semin Radiat Oncol. 2001; 11(1):47–57. [PubMed: 11146042]
11. Baudelet C, Gallez B. How does blood oxygen level-dependent (BOLD) contrast correlate with oxygen partial pressure (pO2) inside tumors? Magn Reson Med. 2002; 48(6):980–986. [PubMed: 12465107]
12. Zhao D, Jiang L, Hahn EW, Mason RP. Comparison of 1H blood oxygen level-dependent (BOLD) and 19F MRI to investigate tumor oxygenation. Magn Reson Med. 2009; 62(2):357–364. [PubMed: 19526495]
13. Howe FA, Robinson SP, McIntyre DJ, Stubbs M, Griffiths JR. Issues in flow and oxygenation dependent contrast (FLOOD) imaging of tumours. NMR Biomed. 2001; 14(7–8):497–506. [PubMed: 11746943]
14. Zhao D, Constantinescu A, Jiang L, Hahn EW, Mason RP. Prognostic radiology: quantitative assessment of tumor oxygen dynamics by MRI. Am J Clin Oncol. 2001; 24(5):462–466. [PubMed: 11586097]
15. Zhao D, Jiang L, Mason RP. Measuring changes in tumor oxygenation. Methods Enzymol. 2004; 386:378–418. [PubMed: 15120262]
16. Mason RP, Ran S, Thorpe PE. Quantitative assessment of tumor oxygen dynamics: molecular imaging for prognostic radiology. J Cell Biochem Suppl. 2002; 39:45–53. [PubMed: 12552601]
17. Jordan BF, Cron GO, Gallez B. Rapid monitoring of oxygenation by 19F magnetic resonance imaging: Simultaneous comparison with fluorescence quenching. Magn Reson Med. 2009; 61(3): 634–638. [PubMed: 19097235]

18. Kodibagkar VD, Wang X, Mason RP. Physical principles of quantitative nuclear magnetic resonance oximetry. Front Biosci. 2008; 13:1371–1384. [PubMed: 17981636]
19. Mason RP, Antich PP, Babcock EE, Gerberich JL, Nunnally RL. Perfluorocarbon imaging in vivo: a 19F MRI study in tumor-bearing mice. Magn Reson Imaging. 1989; 7(5):475–485. [PubMed: 2607898]
20. Hunjan S, Mason RP, Constantinescu A, Peschke P, Hahn EW, Antich PP. Regional tumor oximetry: 19F NMR spectroscopy of hexafluorobenzene. Int J Radiat Oncol Biol Phys. 1998; 41(1):161–171. [PubMed: 9588931]
21. Robinson SP, Griffiths JR. Current issues in the utility of 19F nuclear magnetic resonance methodologies for the assessment of tumour hypoxia. Philos Trans R Soc Lond B Biol Sci. 2004; 359(1446):987–996. [PubMed: 15306411]
22. Mason RP, Rodbumrung W, Antich PP. Hexafluorobenzene: a sensitive 19F NMR indicator of tumor oxygenation. NMR Biomed. 1996; 9(3):125–134. [PubMed: 8892399]
23. Evans SM, Koch CJ. Prognostic significance of tumor oxygenation in humans. Cancer Lett. 2003; 195(1):1–16. [PubMed: 12767506]
24. Hopf HW, Rollins MD. Wounds: an overview of the role of oxygen. Antioxid Redox Signal. 2007; 9(8):1183–1192. [PubMed: 17536961]
25. Kenmure AC, Murdoch WR, Hutton I, Cameron AJ. Hemodynamic effects of oxygen at 1 and 2 Ata pressure in healthy subjects. J Appl Physiol. 1972; 32(2):223–226. [PubMed: 5007874]
26. Waring WS, Thomson AJ, Adwani SH, Rosseel AJ, Potter JF, Webb DJ, Maxwell SR. Cardiovascular effects of acute oxygen administration in healthy adults. J Cardiovasc Pharmacol. 2003; 42(2):245–250. [PubMed: 12883329]
27. Berry JM, Doursout MF, Butler BD. Effects of hyperbaric hyperoxia on cardiac and regional hemodynamics in conscious dogs. Aviat Space Environ Med. 1998; 69(8):761–765. [PubMed: 9715964]
28. Busing CM, von Gerstenbergk L, Dressler P, Rumm D, Wentz K. Experimental studies on microcirculation under normobaric hyperoxia using the microspheres method. Exp Pathol. 1981; 19(3):146–153. [PubMed: 7250293]
29. Matalon S, Nesarajah MS, Farhi LE. Pulmonary and circulatory changes in conscious sheep exposed to 100% O2 at 1 ATA. J Appl Physiol. 1982; 53(1):110–116. [PubMed: 6811521]
30. Hunjan S, Zhao D, Constantinescu A, Hahn EW, Antich PP, Mason RP. Tumor oximetry: demonstration of an enhanced dynamic mapping procedure using fluorine-19 echo planar magnetic resonance imaging in the Dunning prostate R3327-AT1 rat tumor. Int J Radiat Oncol Biol Phys. 2001; 49(4):1097–1108. [PubMed: 11240252]
31. Perry, RH.; Green, DW. Perry's chemical engineers' handbook. New York: McGraw-Hill; 2008. 1 v. (various pagings) p
32. Barker BR, Mason RP, Bansal N, Peshock RM. Oxygen tension mapping with F-19 echo-planar MR imaging of sequestered perfluorocarbon. J Magn Reson Imaging. 1994; 4(4):595–602. [PubMed: 7949687]
33. Mason RP, Shukla H, Antich PP. In vivo oxygen tension and temperature: simultaneous determination using 19F NMR spectroscopy of perfluorocarbon. Magn Reson Med. 1993; 29(3): 296–302. [PubMed: 8450738]
34. Hou H, Grinberg OY, Taie S, Leichtweis S, Miyake M, Grinberg S, Xie H, Csete M, Swartz HM. Electron paramagnetic resonance assessment of brain tissue oxygen tension in anesthetized rats. Anesth Analg. 2003; 96(5):1467–1472. table of contents. [PubMed: 12707151]
35. Liu KJ, Gast P, Moussavi M, Norby SW, Vahidi N, Walczak T, Wu M, Swartz HM. Lithium phthalocyanine: a probe for electron paramagnetic resonance oximetry in viable biological systems. Proc Natl Acad Sci U S A. 1993; 90(12):5438–5442. [PubMed: 8390665]
36. Thomas SR, Pratt RG, Millard RW, Samaratunga RC, Shiferaw Y, Clark LC Jr, Hoffmann RE. Evaluation of the influence of the aqueous phase bioconstituent environment on the F-19 T1 of perfluorocarbon blood substitute emulsions. J Magn Reson Imaging. 1994; 4(4):631–635. [PubMed: 7949694]
37. Glockner JF, Chan HC, Swartz HM. In vivo oximetry using a nitroxide-liposome system. Magn Reson Med. 1991; 20(1):123–133. [PubMed: 1658535]

38. O'Hara JA, Khan N, Hou H, Wilmo CM, Demidenko E, Dunn JF, Swartz HM. Comparison of EPR oximetry and Eppendorf polarographic electrode assessments of rat brain PtO2. Physiol Meas. 2004; 25(6):1413–1423. [PubMed: 15712720]

39. Rink R, Kessler M. Signs of hypoxia in the small intestine of the rat during hemorrhagic shock. Adv Exp Med Biol. 1973; 37A:469–475. [PubMed: 4500058]

40. Shaw AD, Li Z, Thomas Z, Stevens CW. Assessment of tissue oxygen tension: comparison of dynamic fluorescence quenching and polarographic electrode technique. Crit Care. 2002; 6(1):76–80. [PubMed: 11940270]

41. Brezis M, Heyman SN, Epstein FH. Determinants of intrarenal oxygenation. II. Hemodynamic effects. Am J Physiol. 1994; 267(6 Pt 2):F1063–F1068. [PubMed: 7810693]

42. Sato N, Kamada T, Kawano S, Hayashi N, Kishida Y, Meren H, Yoshihara H, Abe H. Effect of acute and chronic ethanol consumption on hepatic tissue oxygen tension in rats. Pharmacol Biochem Behav. 1983; 18 Suppl 1:443–447. [PubMed: 6685303]

43. Maas AI, Fleckenstein W, de Jong DA, van Santbrink H. Monitoring cerebral oxygenation: experimental studies and preliminary clinical results of continuous monitoring of cerebrospinal fluid and brain tissue oxygen tension. Acta Neurochir Suppl (Wien). 1993; 59:50–57. [PubMed: 8310863]

44. Hall LW, Jackson SR. Hexafluorobenzene. Further studies as an anaesthetic agent. Anaesthesia. 1973; 28(2):155–159. [PubMed: 4696356]

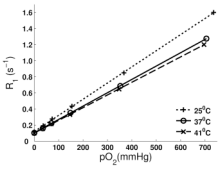


**Fig. 1.**

Linear fits of $R_1$ of HFB (with 2% Isoflurane) vs. $pO_2$ from 0% to 100% at 25°C, 37°C and 41°C. Each sample point represents the mean of 3 individual samples (SD < 0.0153 $s^{-1}$ at all points displayed).

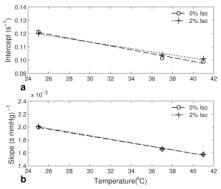


**Fig. 2.**

The dependence of intercept and slope on temperature as depicted from Table 1. Data from calibration with and without the presence of isoflurane are displayed. **a:** Linear fits of intercept vs. temperature according to Eq. [2]. **b:** Linear fits of slope vs. temperature according to Eq. [2].

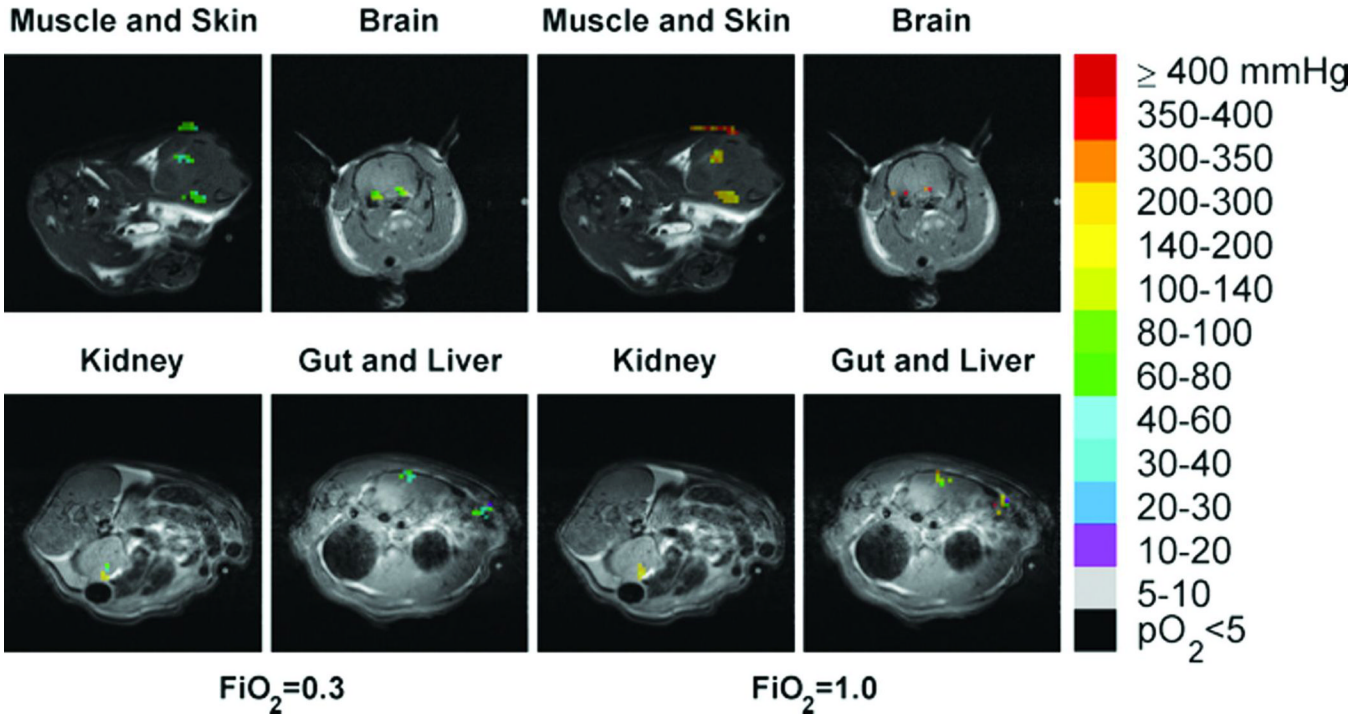


**Fig. 3.**

Tissue oxygen distributions of six organs at $FiO_2$ of 0.3 (left) and 1.0 (right) shown in color superimposed on proton anatomical images shown in black and white. $PO_2$ reference ranges corresponding to different colors are shown on the side bar color key.

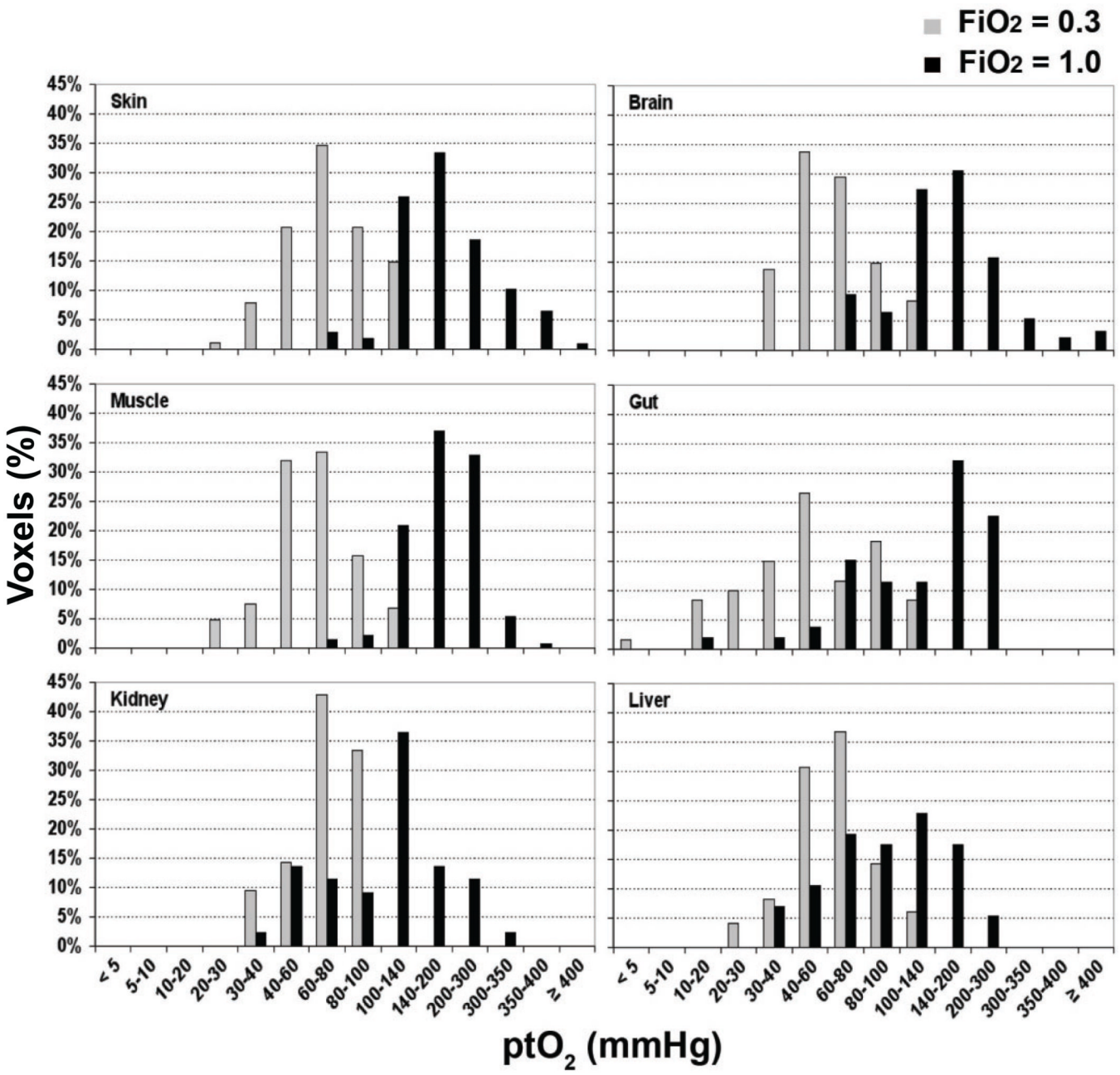


**Fig. 4.**

Separate organ histograms showing the distribution of individual voxel $ptO_2$ values recorded from all 12 animals are displayed at both an $FiO_2$ of 0.3 (gray) and 1.0 (black).

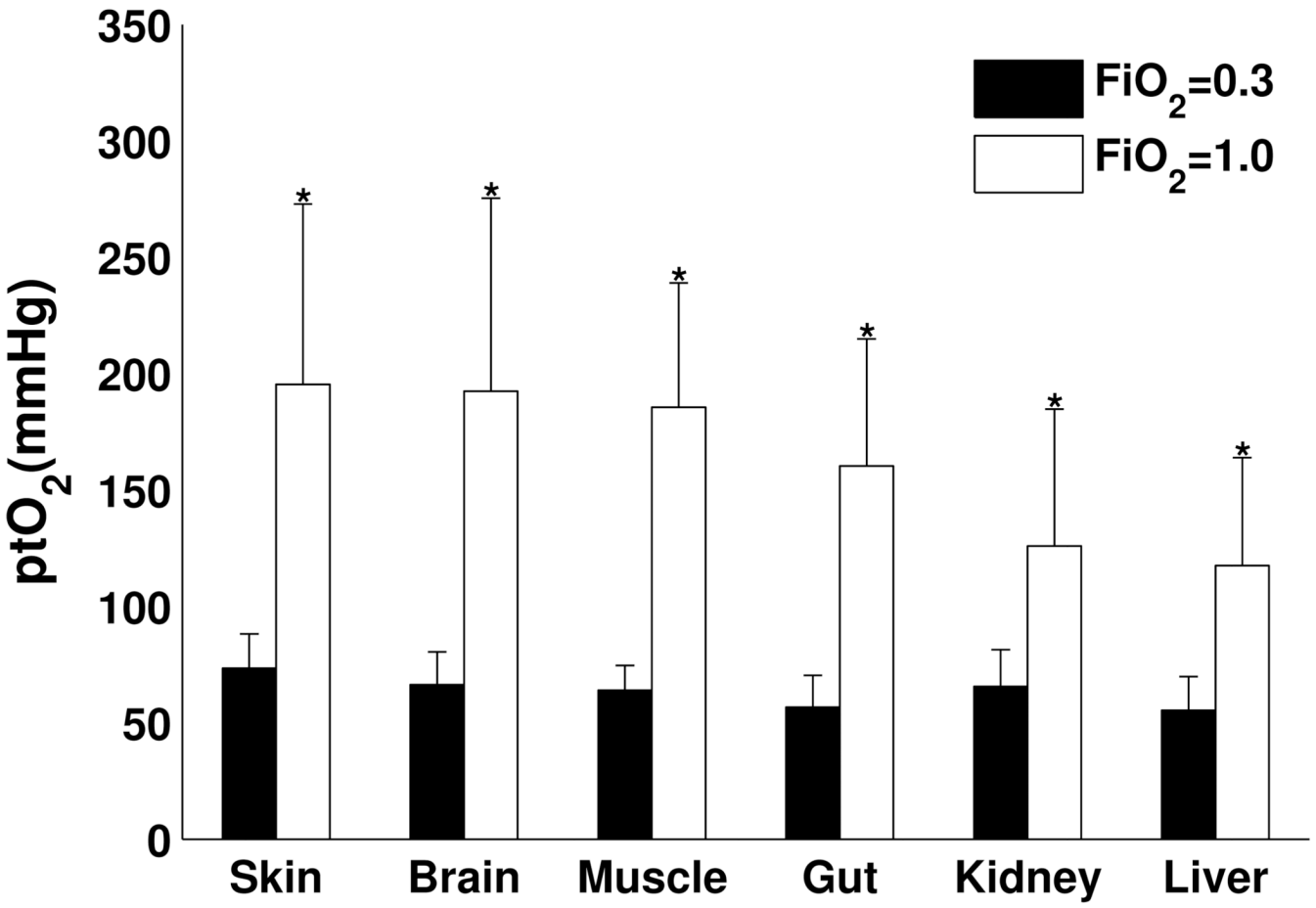


**Fig. 5.**

Bar plots of mean $ptO_2$ over all voxels in brain, kidney, liver, gut, muscle and skin among 12 studied animals at $FiO_2$ of 0.3 and 1.0. Significant differences (*) are noted for all organs as the $ptO_2$ at an $FiO_2$ of 1.0 is significantly increased compared to values at an $FiO_2$ of 0.3 ($p<0.05$).

## Table 1

The intercept and slope obtained from calibration data at 0% or 2% isoflurane at three temperatures

| Isoflurane (%) | Temperature(°C) | Intercept ($s^{-1}$) | Slope $10^{-3}$ $(s\ mmHg)^{-1}$ |
|---|---|---|---|
| 0 | 25 | 0.121 ± 0.004 | 1.997 ± 0.013 |
| 0 | 37 | 0.102 ± 0.003 | 1.658 ± 0.008 |
| 0 | 41 | 0.099 ± 0.003 | 1.576 ± 0.010 |
| 2 | 25 | 0.120 ± 0.004 | 2.008 ± 0.012 |
| 2 | 37 | 0.104 ± 0.001 | 1.659 ± 0.004 |
| 2 | 41 | 0.101 ± 0.002 | 1.578 ± 0.006 |

Data are mean ± SD from three individual samples using the linear fit from Eq. [1]. No significant effect on the intercept or slope from the presence of isoflurane.

## Table 2

Physiological values measured during in vivo experimentation at $FiO_2$ of 0.3 and 1.0

| Physiological Variables | $FiO_2$ = 0.3 | $FiO_2$ = 1.0 |
|---|---|---|
| Arterial $pO_2$ (mmHg) * | 98 ± 12 | 400 ± 85 |
| Arterial $pCO_2$ (mmHg) | 36 ± 5 | 40 ± 4 |
| Hb (g/dL) | 12.8 ± 0.8 | 12.9 ± 0.9 |
| Mean arterial pressure(mmHg) | 90 ± 6 | 86 ± 9 |
| Temperature (°C) | 37.3 ± 0.3 | 37.3 ± 0.6 |
| Heart rate (beats/minute) | 352 ± 38 | 353 ± 23 |

Data are mean ± SD. A significant difference (*) was noted in the arterial $pO_2$ ($p<.001$) between the conditions. No significant difference ($p<.05$) was noted between conditions for the remaining physiologic variables.